RESEARCH ARTICLE

Check for updates

Large-pore mesoporous silica: template design, thin film preparation and biomolecule infiltration†

Sebastián Alberti, [ID] *[a] Sonja Schmidt,[b] Simone Hageneder,[c] Paula C. Angelomé, [ID] [e] Galo J. A. A. Soler-Illia, [ID] [d] Philipp Vana, [ID] [b] Jakub Dostalek, [ID] [cf] Omar Azzaroni [ID] [a] and Wolfgang Knoll[cg]

Nanopores have been applied in the development of artificial biocatalytic systems, controlled drug delivery, and solid-state sensing devices. The interaction of biomacromolecules with surfaces show a dependence on the nanopore diameter, crucial in their ability to infiltrate porous materials. In this context, ordered mesoporous materials obtained by evaporation-induced self-assembly are model materials to test pore-biomolecule interactions. Nevertheless, these materials are generally restricted to pore diameters within the 2–10 nm range, therefore, new polymers as templating agents hold potential to provide an easy reproducible route for the synthesis of mesoporous silica thin films (MTF) with pore diameters above 10 nm without the use of swelling or additional structuring agents. Here, we present a novel and simple approach towards large pore MTF through the combination of supramolecular templating and phase separation with tailor-made block co-polymers. Accurate tuning of the oxide pore size distribution (with small mesopores between 13–18 nm diameter) is achieved by controlling the length and the nature of the hydrophilic polymer block used as a template through a simple reversible addition-fragmentation chain transfer (RAFT) polymerization approach. The importance of these features is highlighted by showing the capability that these new materials offer for biomolecule infiltration benchmarked against the widespread MTF prepared using pluronic F127 as a template. Effect of protein to pore diameter ratio, protein location and effect of pH and ionic strength is briefly tested and discussed.

Introduction

Nanoporous structures, due to their large area-to-volume ratio and confinement effect, have proved themselves ideal as adsorbents for sensing applications, water purification,[1] catalysis,[2–4]

[a] *Instituto de Investigaciones Fisicoquimicas Teoricas y Aplicadas (INIFTA), Departamento de Quimica, Facultad de Ciencias Exactas, Universidad Nacional de La Plata-CONICET, CC. 16 Suc. 4, La Plata, 1900, Argentina. E-mail: sebastian.alberti@uit.no*

[b] *Georg-August-University Göttingen, Institute of Physical Chemistry, Tammannstr. 6, 37077 Göttingen, Germany*

[c] *Biosensor Technologies, AIT-Austrian Institute of Technology, Konrad Lorenz Straße 24, 3430 Tulln, Austria*

[d] *Instituto de Nanosistemas, Universidad Nacional de General San Martín-CONICET, San Martín, 1650, Argentina*

[e] *Instituto de Nanociencia y Nanotecnología & Gerencia Química – Centro Atómico Constituyentes, CNEA-CONICET, Av. Gral. Paz 1499, 1650, San Martín, Buenos Aires, Argentina*

[f] *FZU-Institute of Physics, Czech Academy of Sciences, Na Slovance 2, Prague 182 21, Czech Republic*

[g] *Danube Private University, Steiner Landstrasse 124, 3500 Krems, Austria*

† Electronic supplementary information (ESI) available. See DOI: https://doi.org/10.1039/d3qm00378g

drug delivery,[5] bone regeneration[6] and solid-state nanopore sensing devices.[7] The richness of chemical phenomena in confined environments opens the path to advanced applications that rely on designed substrate–surface interactions.

In particular, its application in nanopore-based biotechnologies is highly sensitive to pore diameter, due to conformation of biomacromolecules and surface interaction in confinement.[8] Optimal nanopore diameters have been reported for enhancing the stability of the folded structures,[9–11] and inhibit irreversible aggregation despite being under protein crowding conditions.[12–14] Furthermore, the knowledge of protein location and assembly within a material will contribute to design programmable or multifunctional bio-composite systems inside nanopores and to make nanopore based sensing of protein structures more accurate.[15,16]

Mesoporous oxide thin films (MTF) provide a sound platform for the creation of ordered arrays of monodisperse cavities. Nowadays, they can precisely designed and produced in reproducible fashion.[17,18] Indeed, the synthesis of MTF by combination of soft chemistry, self-assembly of supramolecular templates (Fig. 2), and surface modification permits to create hybrid interfacial nanoarchitectures where chemical functions

can be precisely located in space.[19–23] Nevertheless, the most common polymers used as porogenic agents limit the preparation of MTF to pore sizes below 10 nm in diameter and rather narrow connecting necks below 5 nm in diameter.[24] In this regard, most reports rely on commercial templating agents such as CTAB, the diblock co-polymer Brij family, and the triblock co-polymer pluronic family.[25] Among them, pluronic F127 gives rise to the biggest pore sizes, with up to 7–8 nm pore diameter and necks below 4 nm.[17] These limited pore sizes can be subsequently further reduced by post-grafting procedures leading to a loss in porous volume, monodispersity and eventually to pore blocking.[26–28] In applications that require coupling delicate macromolecules, such as enzymes, to the inorganic material, the narrow pore size imposes a severe drawback. In particular, immobilization of biomolecules has appeared as a promising field for applications such as catalysis, sensing or soil remediation.[29–31] In this regard, preparing structures with enlarged pore diameters up to 40 nm represents a step forward, since they can accommodate macromolecules without losing the key confinement effects.[8,32] However, expanding mesopores sizes beyond 10 nm diameter while ensuring a high pore volume in an easy and reproducible way without the use of toxic solvents remains a big challenge.

In search of increasing the pore size in mesoporous structures, different groups have approached the problem with several strategies based on the development of specific templating agents, the addition of swelling agents, or the use of nanoparticles as templates.[33,34] The evaporation induced self-assembly (EISA) method is a very flexible and well developed synthesis route,[35] yet so far, large pores using a single templating agent have only been attained in ultrathin oxide films (pore monolayers or bilayers, or even arranged craters) with very dilute precursor concentrations.[36–38] Furthermore, new commercial polymers as porogenic agents are usually limited to polyethylenoxide (PEO) as the hydrophilic block and only very few alternatives have been proposed.[32] These new polymers normally require the use of expensive or toxic solvents that complicate scaling up of the production.[39] The introduction of swelling agents presents an alternative strategy and has been successfully used in several materials, but this strategy adds complexity to the solution composition.[38] Other limitations like thermal treatments, aging time, layer thickness and lack of monodispersity are to be considered when this approach is used.[38] A third approach to widening pore diameters through sol–gel chemistry has been based on the use of nanoparticles as templates, as is the case for latex nanoparticles. This approach mainly leads to macroporous structures (pore diameter above 50 nm) and interconnectivity between the pores may be limited.[34] Despite all these efforts, pore sizes between 15–40 nm have not been achieved in a standard and reproducible manner and a new facile route for pore design within this scale is still needed.[40]

In this regard, novel co-polymers prepared by controlled radical polymerization (CRP) procedures can be used as templates, taking advantage of incorporating a broad spectrum of radically (co)polymerizable monomers.[41] Controlled polymerization strategies (*i.e.* atom transfer radical polymerization (ATRP), nitroxide mediated radical polymerization (NMP) and reversible addition-fragmentation chain transfer polymerization (RAFT)) allow to obtain polymers with low molar mass polydispersity without the need of further purification.[32,42] Furthermore, this technique enables the use of less stringent conditions as those required for anionic polymerization.[43] These procedures allow for the design of a straightforward route for block copolymer synthesis, as polymerization can be stopped and restarted in the presence of a new monomer without the need of further purification. Within CRP, RAFT polymerization provides an easy protocol for block copolymer synthesis with an outstanding control over the length and monodispersity of each block, compatible with commercial monomers (acrylates, methacrylates and styrene).[44] This diversity of functional groups enables the synthesis of tailor-made polymers. Interestingly, these polymers can be used as template agents but also as precursors to functionalize the inner pores.[45]

In this work, we will briefly discuss the design and the synthesis of new triblock co-polymers, soluble in ethanol, to be used as templates for mesoporous silica thin films synthesis through sol–gel chemistry. The ratio of the hydrophobic block volume to the hydrophilic block volume will be tuned by changing the hydrophobic polymer length. In addition, the degree of hydrophobicity will be studied by changing the nature of the respective polymer block. This study gives us the opportunity to find the configuration that will define the pore size and pore volume of the porous films and guarantee a reproducibility that is currently not achievable with the available commercial polymers. These new mesoporous thin films will be compared to a widely known pluronic F127 based MTF. Finally, to demonstrate the possible applications of the obtained materials, we will report a systematic study on biologically relevant proteins infiltration, taking advantage of the wide MTF pore size here synthesized. The effect of pore size, protein molecular weight, protein isoelectric point and solution ionic strength on protein infiltration will also be analyzed, in search of the limiting conditions for infiltration. The design of such material is highlighted as a step forward for the clever design of hybrid materials arising from the integration of entities coming from supramolecular chemistry, macromolecular chemistry, biochemistry and material science.

Results and discussion

Co-polymer synthesis and MTF preparation

The synthesis of triblock co-polymers to be used as template agents was done through RAFT polymerization which requires the presence of thiocarbonylthio compounds,[46] such as dithioesters, thiocarbamates, and xanthates known as chain transfer agents (CTAs). These agents carry R- or Z-groups to mediate the polymerization *via* a reversible chain-transfer process. In the present work, a symmetric trithiocarbonate CTA, diethyl 2,2′-(thiocarbonylbis(sulfanediyl))bis(2-methylpropanoate), with two equivalent R groups was chosen for the two step synthesis of
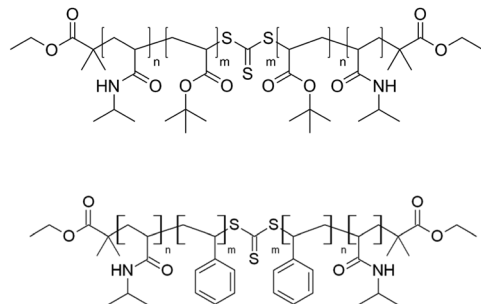
Fig. 1 PN-PB and PN-PS polymers structures.

triblock co-polymers (Fig. S1, ESI†). The length of the macro RAFT agent, *i.e.* the length of the final outer blocks, was kept constant and the length of the hydrophobic inner blocks was varied to modify the head to tail ratio. These structural parameters allowed to tune the self-assembly process and thus the size of the micelle to which the polymer self assembles.

As a final product three *N*-Isopropylacrylamide (NIPAM)-*t*butylacrylate-NIPAM co-polymers (named PN-PB-12, PN-PB-24 and PN-PB-48) and other three PNIPAM-polystyrene-PNIPAM co-polymer (named PN-PS-12, PN-PB-24 and PN-PS-48) were obtained (see molecular structures in Fig. 1). Table S1 (ESI†) summarizes the block length and the molecular weight of the obtained polymers.

The prepared triblock co-polymers were analyzed by thermogravimetric analysis (TGA) and compared to the commercial polymer Pluronic F127 (Fig. S2, ESI†). Pluronic F127 burns completely at 230 °C while PN-PB start to decompose at 270 °C and PN-PB at 340 °C. The residue amount decreases even further towards higher temperatures, burning completely at temperatures close to 500 °C.

Each new block co-polymer was used as a templating agent to produce mesoporous SiO$_2$ thin films. To this end, polymers were added to ethanol solutions of prehydrolized TEOS, ethanol and hydrochloric acid. Sols showed a colorless clear appearance in all cases. Nevertheless, it should be noted that high molecular weight hydrophobic blocks (polymers PN-PB-48 and PN-PS-48) presented limited solubility under the tested conditions. The increase in the hydrophobic-block molecular weight lowers polymer solubility and therefore the amount of template dissolved limits the pore volume, as will be discussed later.

The sols were spun onto glass substrates and thermally treated to obtain the mesoporous oxides (Fig. 2). The thermal treatment was chosen according to TGA results. Although the polymers are completely decomposed above 500 °C, when they are used as templating agents, the effect on the oxide structure should be taken into account. Due to their curvature and thin wall thickness, mesoporous materials are sensitive to temperature, and sintering occurs approaching 500 °C, affecting the porous structure (see Fig. S3, ESI†). Therefore, a temperature above 370 °C (burning temperature of PN-PS and the second drop in mass for PN-PB) and below 500 °C was chosen for calcination. Calcination was done at 400 °C for two hours, the total amount of residues left was below 25% and 10% for PN-PB and PN-PS respectively.

The surface of the thin films obtained was analyzed by Scanning Electron Microscopy (SEM). SEM images, presented in Fig. 2, show a great variety of pore morphology ranging from low to high polydispersity and well-defined and shapeless pores. The information is summarized in the histograms in Fig. 2. Statistical analysis of the SEM images was performed to estimate pore distribution and mean pore size of each sample. Additionally, thin films were studied through ellipsometry at
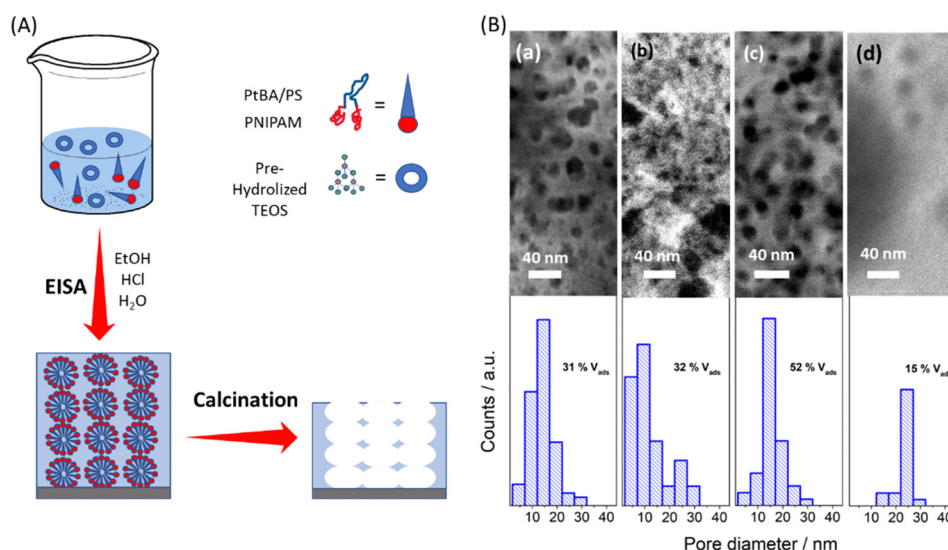

Fig. 2 (A) On the left scheme of the synthesis of the MTF. (B) Histogram showing pore distribution based on SEM images for MTF based on the synthesized templates: PN-PB-24 (a), PN-PB-48 (b). PN-PS-12 (c), PN-PS-24 (d). The surface was homogenous though the whole sample, pore count ranges from 25 to 110 depending on the pore density. Pore volume was calculated through ellipsometry measurements at 0 and 100% humidity.

4144 | *Mater. Chem. Front.*, 2023, **7**, 4142–4151

This journal is © The Royal Society of Chemistry and the Chinese Chemical Society 2023

0 and 100% humidity to estimate the pore volume accessible to water vapor.

The two different PN-PB templates (Fig. 2c and d, respectively) allowed for the creation of a MTF with highly monodisperse porosity, with a pore diameter that increased with the molecular weight. The template PN-PB 48 presents a larger hydrophobic block compared to PN-PB 24, while both PN-PB-24 and PN-PB-48 were designed to achieve a 2–3 fold higher molecular weight compared to PN-PB-12 (see Fig. S4 and Table S1, ESI†). This increment in polymer weight was reflected in an increase of the pore size and porous volume, leading to a 16 nm mean pore size in the case of PN-PB-24 and 24 nm pore diameter for PN-PB-48. In this latter case, the length of the hydrophilic block was two times the hydrophobic block length and thus the film presented a limited pore volume due to poor interconnectivity. This was attributed to a decrease in solubility as the hydrophobic chain increases, limiting the pore size attainable by this strategy. In the case of PN-PS polymers, well defined pores were obtained for the MTF based on PN-PS-12 with the smallest molecular weight, with general features similar to those of PN-PB-24 (both with similar molecular weight and tail to head ratio), a pore volume of 31% and a pore diameter of 15 nm. PN-PS-24 MTF, with a higher hydrophobic: hydrophilic block ratio, presented a sponge-like structure with poorly defined pores and wide pore size distribution. For this case, undefined micelles are responsible for the pore structure, and undefined aggregates act as molecular spacers. The increase of the hydrophobic block decreases solubility dramatically, and the hydrophobic–hydrophilic balance reaches its solubility limits, preventing any pore structure formation for PN-PS-48.

This variety on pore morphology accounts for several aspects regarding hydrophobicity, solubility, block molecular volumes, and micelle surface area, as described briefly by Israelachivili.[47] A quantitative study would need a meticulous analysis on each of these variables and the dynamic aspect such as the mesostructure organization, inorganic condensation, and the thermal treatments. However, a qualitative analysis can be done taking into account thermodynamic, geometric and kinetic aspects. From a kinetic point of view, small molecules organize swiftly, giving rise to more organized structures and therefore less polydispersity. In contrast, bigger molecules need more time to self-assemble, in an extreme case working as molecular spacers. On the other hand, from a thermodynamic point of view, the hydrophobic/hydrophilic balance is crucial for the phase separation process. Solubility on ethanol of the high molecular weight hydrophobic blocks significantly limits the chances of creating homogenous thin films with high pore interconnection and with high pore volume. Low solubility entails low amounts of template molecules and compromises the mesoporous thin films formation, giving rise to spread-out pores and poor connectivity as seen in the case of PN-PB-48. In the worst-case scenario, no pores are found for the final films as for PN-PS-48. In a more detailed analysis, geometrical parameters should be considered, as well. The molecular volume of both the tail (hydrophobic) and the head (hydrophilic) of the

synthesized polymers are one of the main features that define micelle size and mesophase morphology and are computed into a parameter known as compact factor. As the ratio of hydrophobic to hydrophilic volume increases pore size, eventually, globular, cylindrical, and lamellar mesophases could be formed.[35]

MTF-PN-PB-24 Comparison to MTF-F127

According to the results and the discussion presented in the last section, PN-PB-24 showed the best performance as a porogenic agent for creating MTF with pore sizes above 15 nm. PN-PB-24-based MTF leads to highly interconnected pores, with a porous volume above 50%. This outstanding new MTF was chosen for further characterization and comparison with mesoporous thin films obtained through commercial block co-polymer, Pluronic F127, commonly used in the literature.[18,24,25] SEM images, environmental ellipsometric porosimetry (EEP), X-ray reflectometry (XRR) at 0 and 100% humidity, and grazing incidence small angle X-ray scattering (GI-SAXS) for both thin films are shown and compared in Fig. 3 and 4, respectively. Additional AFM and SEM cross section of PN-PB-24 templated films are presented in Fig. S5, ESI.†

As can be seen from the SEM images, pores sizes for films obtained using PN-PB-24 are much wider than the ones obtained with Pluronic F127, a mean diameter size of 17 nm is obtained in contrast to a mean size of 7 nm for the commercial polymer; this results matches perfectly with pore size distribution measured by EEP and relate to a surface area of 380 m² g⁻¹ and 270 m² g⁻¹ measured following BET model. XRR measurements (Fig. 4a and b) show well-defined Kiessig
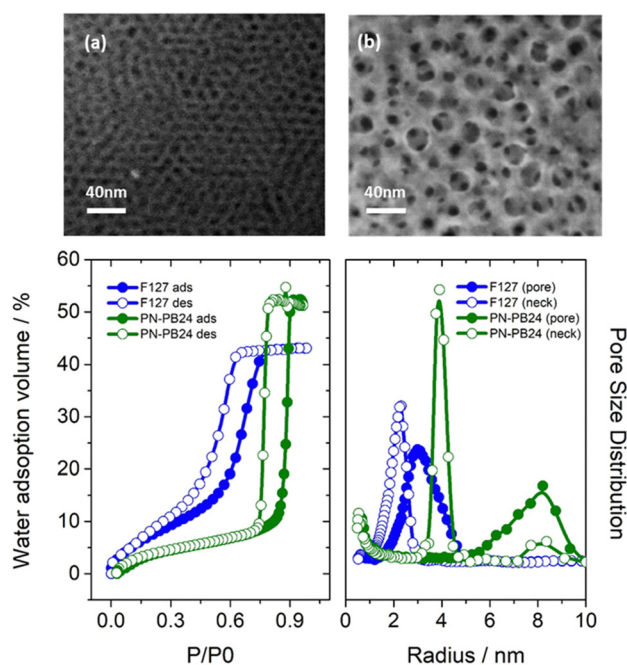

Fig. 3 SEM analysis of the films surface for MTF–F127 (a) and MTF-PB-PB-24 (b) samples. EEP isotherm (b) and pore distribution analysis (c) for MTF-PN-PB-24 (green) and MTF-F127 (blue)
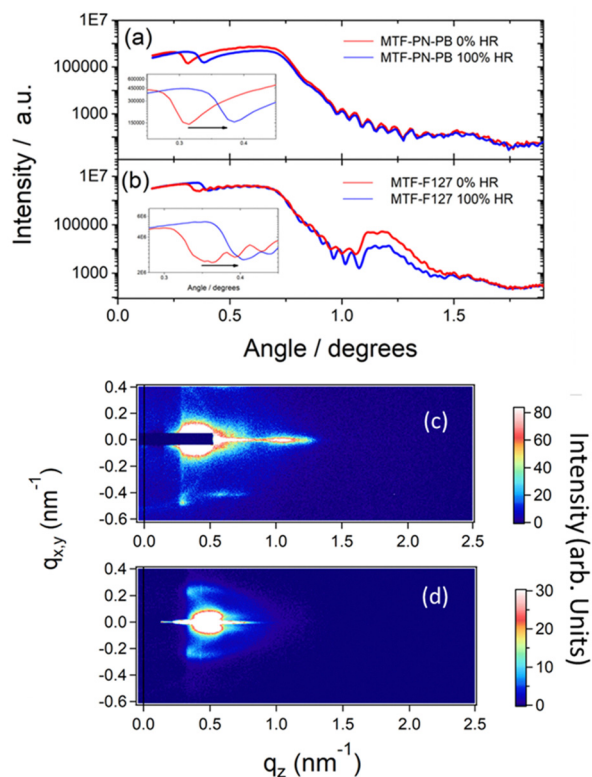
Fig. 4 X-ray Reflectometry results obtained at low and high RH for (a) MTF-PN-PB-24 and (b) MTF-F127. Insets: Critical angle displacement upon water adsorption. GI-SAXS patterns for (c) MTF-F127 and (d) MTF-PN-PB24.

fringes for both films exhibiting smooth surfaces and thickness was calculated to be approximately 200 nm and 300 nm for MTF-F127 and MTF-PN-PB-24, respectively. XRR measurements performed at 0% RH and 100% RH confirm a porous volume accessible to water above of 50% for MTF-PN-PB-24 sample. These results are in agreement with the data acquire by EEP measurements which shows a porous volume of 53% and 45% for MTF-PN-PB-24 and MTF-F127, respectively. Additionally, interplanar distance of 7 nm along the Z-axis could be calculated from XRR for MTF-F127 sample. Data from MTF-PN-PB-24 samples show a much less clearly defined interplanar distance along the Z-axis of 15 nm.

Finally, GI-SAXS measurements (Fig. 4c and d) confirm a more ordered structure for the F127 templated sample. This sample presents a uniaxially contracted body centered cubic $Im3m$ mesostructure, as reported elsewhere.[48] The MTF-PN-PB-24 sample, on the other hand, shows a local order but not an as well-defined structure as the F127 based ones, in agreement with XRR measurements. Nevertheless, these measurements allow to calculate interplanar distances within the X-Y-plane for both systems, being 26,6 nm and 12,2 nm for PN-PB-24 and F127, respectively. It is worth noting that interplanar distances within X-Y plane are much larger (around 70% larger) than those perpendicular to the Z axis due to contraction in Z direction after thermal treatments, typical of mesoporous thin films (Fig. S5, ESI†).[48]

Biomolecules infiltration

While mesoporous silica was demonstrated to be a compelling candidate for the implementation of biotechnological applications requiring protein confinement and immobilization, the understanding of protein behavior upon physical adsorption into silica pores is limited. Infiltration of proteins and, in particular, enzymes into porous structures has been exploited as a key strategy for sensing purposes, biocatalyst platforms[49] or fuel cells.[30,50,51] Furthermore, encapsulation of enzymes has been seen as an outstanding way to improve enzyme stability[52] and was exploited for catalytic purposes and even soil or water remediation.[53] From another perspective, the possibility to avoid protein infiltration may give these materials the ability to sieve small molecules from complex solution, such as blood or saliva, for sensing purposes.[54]

Infiltration of macromolecules has been described previously by several authors[55-57] by indirect methods to assess general adsorbed protein, such as Fourier-transform infrared spectroscopy and activity assays or depletion from solution. However, the limitation of these methods to distinguish spatial protein arrangement within the pores and the outer surface compromise future applications. In particular, Caruso's and Jiskoot's groups studied infiltration of proteins in mesoporous particles,[33] nevertheless their study based on silica particles has spatial resolution limitations. MTF open the door to specific characterization techniques able to discriminate between the deposition of molecules inside the pores from the deposition on the top surface of the film through widely available techniques such as ellipsometry, XRR or optical waveguide spectroscopy (OWS).

In this work, infiltration of biomolecules within MTF was carried out to analyze the potentialities of the new wide pores. For this purpose, a concise infiltration study was performed in MTF-PN-PB-24, and similar studies were done on MTF-F127 for comparison purposes. Multi-mode OWS, through a careful study of the changes of the guided modes in the thin film, allows us to distinguish infiltration of proteins to the outer interface due to the refractive index change in distinct layers (examples and more details are provided in Fig. S6 and S7, ESI†).[58] Thus, OWS is the technique of choice for a systematic study on the infiltration of biologically relevant proteins in mesoporous thin layers.

Five proteins of different molecular weights with isoelectric points above 5 were selected to test the infiltration: adenosine deaminase, neutravidin, glutaminase, amino acid oxidase, and urease. The influence of ionic strength and isoelectric point was taken into account to determine the best conditions for infiltration (see Table S2, ESI†). The isoelectric point was carefully selected to be above the working pH, since this will determine a positive protein charge and avoid charge exclusion to hinder any protein infiltration. Lactalbumin is used to test the importance of the isoelectric point in the infiltration: at Ph = 7 lactalbuminis negatively charged and, despite its small size, is not able to infiltrate.

Additionally, we prove that an increase in ionic strength may favor protein infiltration (Table 1 and Table S2, ESI†), in

Table 1 Change in refractive index of MTF-PN-PB-24 and in the thickness of the polymer layer on top. Characteristic data of the enzymes is added for comparison

Protein	Molecular weight (kDa)	Isoelectric point	pH	Buffer	ΔRefractive index	ΔThickness (nm)	Diameter range (nm)
Lysozyme	14	10	5	PBS	0.061 (27% pore filling)	5	3–5
Neutravidin	66	6.3	4.5	PBS	0.023 (10% pore filling)	10	4–6
Glutaminase	110	5.4	4.5	PBS	0.024 (10% pore filling)	6	6–10
Amino acid oxidase	110	6.3	4.5	PBS	0.026 (11% pore filling)	7	5–11
Urease	440	5.2	4.5	PBS	0.008	23.3	14–20

Table 2 Change in refractive index of MTF-F127 and in the thickness of the polymer layer on top. Characteristic data of the enzymes is added for comparison

Protein	Molecular weight (kDa)	Isoelectric point	pH	Buffer	ΔRefractive index	ΔThickness (nm)	Diameter range (nm)
Lysozyme	14	10	5	PBS	0.012 (7% pore filling)	23	3–5
Lysozyme	14	10	5	PBSx 10^{-1}	−0.01	10	3–5
Lactalbumin	14	4	7	PBS	−0.003	0	2–4
Neutravidin	66	6.3	4.5	PBS	−0.009	5	4–6

agreement with work reported by Lazzara *et al.* and Caruso's group.[58,59] The results are summarized in Table 1 for the system MTF-PN-PB-24 and Table 2 for system MTF-F127. It is worth noticing that for MTF-F127 the smallest enzymes were studied (lysozyme, lactalbumin and neutravidin) as no infiltration occurs for larger molecules.

The results show that proteins above 110 kDa are not able to infiltrate MTF-PN-PB-24 porous matrix. In contrast, all proteins are adsorbed on top of the MTF layer, with a layer thickness that increases as the molecular weight becomes larger. This tendency is disrupted by neutravidin, for this protein the overlayer thickness doubles the molecule size. Although the model parameters (refractive index of the porous layer and thickness of the overlayer) is limited to the number of guided modes (TM_0 and TE_0) and no gradient can be modeled, this anomalous result may account for some protein infiltration in the pores close to the surface, before a complete pore blocking. This results are in agreement with recent publication on myoglobin infiltration and condensation at pores entrance.[13,60] Results of infiltration of glutaminase and amino acid oxidase show an increased overlayer deposition close to the enzyme diameter. In case of urase the infiltration into the structure seems to be hindered and an overlayer thickness similar in value to the enzyme diameter was measured.

Infiltration of proteins through MTF-F127 layers is only feasible for low molecular weight proteins. Lysozyme does not infiltrate the whole pore structure (pore filling 7%) as could be seen for MTF-PN-PB-24 (pore filling 27%), nevertheless, the protein layer thickness triples the enzyme mean diameter value. Therefore, we can argue that the enzyme infiltrates the first layer of pores before a complete blockage. In the same way as described for neutravidin in the MTF-PN-PB-24 system, here we are in the presence of a limiting case where infiltration is hindered partially and limited to the superficial pores. Therefore, bigger proteins are not be able to infiltrate the structure. This assumption is supported by the inability of neutravidin to infiltrate. These results clearly demonstrate that

the preparation of mesoporous thin films with wider pores give rise to more accessible materials for macromolecules and biomolecules incorporation, as exemplified here with protein infiltration.

Experimental

Materials

N-Isopropylacrylamide (NIPAM, TCI-Chemicals, 97%), and 2,2′-Azobis-(methylpropionitrile) (AIBN, Akzo Nobel, 98%) were recrystallized twice from toluene/hexane (3 : 1) and methanol and dried. *tert*-Butylacrylate (ᵗBA) and styrene (St) were purchase from Sigma Aldrich and passed through a basic aluminum oxide column before use. All other chemicals were obtained from commercial sources and used without further purification. Diethyl 2,2′-(thiocarbonylbis(sulfanediyl))bis(2-methylpropanoate) was synthesized following a procedure published earlier[46] using ethanol instead of butanol as solvent. Ethanol, pluronic F127, tetraethyl ortosilicate (TEOS), hydrochloric acid, Potassium hydroxide, were purchased from Sigma-Aldrich. Ultrapure water (Resistivity = 18 MΩ cm⁻¹) was used in all of the experiments.

Neutravidin was obtained from Thermo scientific, glutaminase (40%) from Sorachim, D-amino acid oxidase (90%) from Calzyme, and Urease from Canavalia ensiformis (Jack Bean) type IX (50 000–100 000 units per g), lactalbumin form bovine milk (85%) and Lysozyme (98%) were provided by Sigma-Aldrich.

Methods

General procedure for the template synthesis. The RAFT agent (CTA), NIPAM, AIBN and DMF were introduced in a reaction vial sealed with a septum (see Table S1 for quantity of reagents, ESI†). The polymerization solution was deoxigenated bubbling argon during 20 min on ice. The vial was taken to a 70 °C heating block to polymerize for 24 hours. The resultant solutions were precipitated twice in cold diethylether

(Fig. S1, ESI†). Molecular mass was determined through size exclusion chromatography (SEC). This polymer will become the macro-RAFT agent used on the following polymerization.

Synthesis of the hydrophobic block. The macroRAFT agents, AIBN, *tert*-butyl acrylate or styrene, were dissolved in DMF (see Table 1). The solution was degassed bubbling argon for 20 minutes on ice and divided in three aliquots. The solution was taken to a 60 °C bath for 12, 24 and 48 hours (Fig. S1, ESI†). The resultant solution was precipitated on hexane. SEC analysis reveals monomer conversion and the molecular weight. The ratio between monomer was studied through Nuclear Magnetic Resonance (NMR).

Nuclear magnetic resonance. Spectra were measured with a Varian Unity 300 instrument, using deuterated dichloromethane as solvent. The spectra were calibrated to the residual signal of the solvent.

Size exclusion chromatography. Characterization of all polymer samples was performed with DMAc containing 0.1% (w/w) of lithium bromide as the eluent using an Agilent 1260 Infinity system, composed with an autosampler, an isocratic solvent pump, a PSS GRAM (polyester co-polymer network) precolumn (8×50 mm), three PSS GRAM separation columns (8×300 m, nominal particle size $= 10^{-5}$ m; pore sizes $= 30$, 10^3, and 10^3 Å) maintained at 45 °C in a column compartment, a 80 Hz UV detector (set to a wavelength of 310 nm for the RAFT polymers), and a refractive index (RI) detector. The flow rate of the mobile phase was 8×10^{-4} L min^{-1}. The whole setup was calibrated with a total of 12 PSS/poly(methyl methacrylate) standards ($M_n = 0.8 - 1820$ kg mol^{-1}) of low dispersity with toluene as internal standard. All samples were filtered through a 450 nm PTFE syringe filter prior to injection. The concentration of the polymer samples was 3 g L^{-1}.

Thermogravimetry Analysis (TGA). Thermal stability of the polymers was studied on a Netzsch TG 209 F3 Tarsus equipment from ambient temperature to 1000 °C with a heating rate of 10 °C min^{-1} under an air flow of 10 mL min^{-1}.

Sols and thin films preparation. Sols were prepared under continuous stirring. Prehydrolized TEOS[61] was added to ethanol, subsequently the templating agent and acidic water were incorporated. The final molar ratios for MTF-F127 sol was: 1 TEOS : 0.005 F127 : 40 EtOH : 10 H$_2$O : 0.01 HCl. The solution was aged during two days prior to film preparation. New polymer - sols solution were prepared by replacing pluronic F127 for the synthesized polymers. The tested final composition were: 1 TEOS : X PNIPAM-*b*-P^{t}BA-*b*-PNIPAM : 40 EtOH : 10 H$_2$O : 0.01 HCl and 1 TEOS : X PNIPAM-*b*-P^S-*b*-PNIPAM : 40 EtOH : 10 H$_2$O : 0.01 HCl, with X between 0.003 and 0.004 depending on the molecular weight; the mass was kept constant for the different polymers.

MTF were synthesized by spin coating the corresponding sol at 1500 rpm for 1 minute over glass substrates. After deposition, the films were subject to a thermal treatment as follows: 60 °C for 30 minutes, 130 °C for another 30 minutes and finally at 400 °C for 2 hours, achieved with a temperature ramp of 3 °C per minute.

Ellipsometry. Film thickness and refractive index were measured using a SOPRA GES5A spectroscopic ellipsometer. Measurement of the ellipsometric parameters Φ (Phi) and Δ (Delta) were carried out under dry nitrogen flux in order to avoid water condensation within the mesopores or under controlled humidity (up to 100% relative humidity). For F127 and PN-PB templated MTF, samples of choice, a complete isotherm was measured. The measured Φ and Δ were satisfactorily fitted with a one-layer model. A Brüggemann effective medium approximation (BEMA) was used to determine the pore volume fraction (V_{pore}/%) from the refractive index values, considering two phases made up of silica ($n_{633nm} = 1.455$) and void pores ($n = 1$).

Optical waveguide spectroscopy (OWS). For these measurements, the MTFs were attached to gold-coated glass substrate made of LASFN9 glass. These substrates were cut to a size of 20×20 mm and cleaned thoroughly in a 2% solution of Hellmanex in water under sonication and subsequent rinsing with water and isopropanol. Vacuum thermal evaporation (HHV AUTO 306 from HHV LTD) in vacuum better than 10^{-6} mbar was used for the subsequent deposition of 2 nm of Cr and 50 nm of Au. After thin film deposition, the gold-coated substrates were stored in argon atmosphere or immediately used for deposition of MTF.

Measurements were performed using a home-built optical instrument relying on Kretschmann configuration utilizing attenuated total reflection (ATR) configuration. It relies on the resonant optical excitation of surface plasmons (SPs) and dielectric OW modes at the sensor surface. Shortly, linearly polarized monochromatic light from a He–Ne laser (PL610P, Polytec, Germany, power 2 mW, wavelength $\lambda = 632.8$ nm) was made passing through a chopper (Princeton Applied Research, USA) and a polarizer, and was coupled to a LASFN9 prism. Onto the prism base, a LASFN9 glass substrate with a 2 nm layer of Cr and 50 nm thick layer of Au was optically matched using immersion oil (Cargile, USA). A flow-cell consisting of a rubber o-ring and a glass substrate with drilled inlet and outlet ports was pressed against the MTF surface to form a chamber with approximately 250 µl volume.

The intensity of the light beam reflected at the prism base was measured using a photodetector and a lock-in amplifier (Model 5210, Princeton Applied Research, USA). The angle of incidence of the light beam was controlled using a rotation stage (Hans Huber AG, Germany). Thereby, the intensity of the light was recorded as a function of the angle of incidence in order to monitor changes in the excitation of surface plasmons (SPs) and optical waveguides modes (OWMs). These modes can be seen as dips in the recorded spectrum in transverse magnetic (TM) polarization for SPs, set by the polarizer, and in both, transverse electric (TE) or transverse magnetic (TM) polarization for OWMs. The readout signal was recorded using Winspall software developed at the Max Planck Institute for Polymer Research, Mainz, Germany.

Grazing-incidence small angle X-ray scattering (GI-SAXS). Measurements were done with a XEUSS 1.0 (XENOCS, Grenoble) instrument with a X Ray source GNIX 3D micro focus and a

4148 | *Mater. Chem. Front.,* 2023, **7**, 4142–4151

This journal is © The Royal Society of Chemistry and the Chinese Chemical Society 2023

PILATUS detector 100 k (Dectris). The sample/detector distance was 1348 mm.

X-ray reflectometry (XRR). Experiments were carried out with a Panalytical Empyrean diffractometer using Cu Kα radiation (λ = 1,54 Å), a 0.38 mm slit and a 10 mm mask. The critical angle was determined at both 5–10% and 90–95% relative humidity, and the accessible porosity was determined from the displacement of this parameter.[62]

Protein infiltration. Glass substrates with 2 nm Cr and 50 nm Au were covered with silica thin films deposited by spin coating at 1000 rpm. The samples were analysed by OWS at TE and TM polarization before and during immersion in a solution of the selected protein in PBS buffer (0.5 mg ml^{-1}). PBS buffer was composed of 140 mM NaCl, 10 mM phosphate buffer, and 3 mM KCl. The immersion was done for 20 minutes, rinsed with distilled water two times and dried under a stream of nitrogen. All measurements were done under nitrogen atmosphere before and after the infiltration.

Scanning electron microscopy (SEM). SEM measurements were carried out in a Field Emission SEM ZEISS LEO 982 GEMINI. Pore structure, pore size and thin layer thicknesses were analysed with ImageJ software.

Conclusions

In this work, we employed RAFT polymerization to develop new porous materials paving the way for the design of silica-based materials with new pores size and pore morphologies. Triblock co-polymer synthetized in work are able to grant a high pore volume, pore diameter above 15 nm and high interconnectivity to mesoporous silica, difficult to achieve using other strategies or commercial attainable block copolymers. This new MTF system have proven to be of high interest for coupling mesoporous materials to macromolecular or biologic entities as enzymes through infiltration, while MTF-F127 based scaffolds present limitations to such applications due to its small pore size. In particularly, it was demonstrated that, the limit of molecular weight for protein infiltration would be approximately 15 kDa for MTF-F127 and 110 kDa for MTF-PN-PB-24.

The results presented in this work should be taken into account for the future design of porous scaffolds for sensors,[63] catalysis,[64] fuel cells[50] and soil remedation[31] that required enzyme, protein or other macromolecule infiltration. In particular, the information presented is highly relevant for both, encapsulation and sieving purposes of porous silica coatings. Although activity of the enzymes studied has not been tested in this work, the presented results provide the foundation for understanding the relation between infiltration and enzymatic activity, as has been exemplified in a recent work.[54]

In summary, this work is an example of rational design implemented in the synthesis of new porous materials and biohybrid materials starting from the template design to the infiltration of macromolecules for potential applications. Two different pathways for functionalizing pores can be ascertained from this work. In the first case we expanded the strategies for custom made block co-polymers to be used for tailor made functionalization of hybrid thin films.[65] In the second, after template removal, infiltration of macromolecules provides the functionalization required.

Author contributions

Conflicts of interest

There are no conflicts to declare.

Acknowledgements

Notes and references

1 P. C. Angelomé and G. J. de A. A. Soler-Illia, Organically Modified Transition-Metal Oxide Mesoporous Thin Films and Xerogels, *Chem. Mater.*, 2005, **17**, 322–331.

2 S. Pariente, P. Trens, F. Fajula, F. Di Renzo and N. Tanchoux, Heterogeneous catalysis and confinement effects, *Appl. Catal., A*, 2006, **307**, 51–57.

3 C. H. Lee, T. S. Lin and C. Y. Mou, Mesoporous materials for encapsulating enzymes, *Nano Today*, 2009, **4**, 165–179.

4 M. B. Majewski, A. J. Howarth and P. Li, Michael R. Wasielewski, J. T. H. & Farha, O. K. Enzyme encapsulation in metal–organic frameworks for applications in catalysis, *CrysEngComm*, 2017, **19**, 4082–4091.

5 S. Alberti, G. J. A. A. Soler-Illia and O. Azzaroni, Gated supramolecular chemistry in hybrid mesoporous silica nanoarchitectures: controlled delivery and molecular transport in response to chemical, physical and biological stimuli, *Chem. Commun.*, 2015, **51**, 6050–6075.

6 M. Vallet-Regi and E. Ruiz-Hernandez, Bioceramics: From bone regeneration to cancer nanomedicine, *Adv. Mater.*, 2011, **23**, 5177–5218.

7 A. Oukhaled, L. Bacri, M. Pastoriza-gallego, J. Betton and J. Pelta, Sensing Proteins through Nanopores: Fundamental to Applications, *Chem. Biol.*, 2012, **7**, 1935–1949.

8 L. Bayne, R. V. Ulijn and P. J. Halling, Effect of pore size on the performance of immobilised enzymes, *Chem. Soc. Rev.*, 2013, **42**, 9000–9010.

9 K. C. Kao, T. S. Lin and C. Y. Mou, Enhanced activity and stability of lysozyme by immobilization in the matching nanochannels of mesoporous silica nanoparticles, *J. Phys. Chem. C*, 2014, **118**, 6734–6743.

10 T. Masuda, *et al.*, Effect of Cavity Size of Mesoporous Silica on Short DNA Duplex Stability, *Langmuir*, 2018, **34**, 5545–5550.

11 S. Satpathi, K. Das and P. Hazra, Silica nano-channel induced i-motif formation and stabilization at neutral and alkaline pH, *Chem. Commun.*, 2018, **54**, 7054–7057.

12 A. Vinu, M. Miyahara and K. Ariga, Assemblies of Biomaterials in Mesoporous Media, *J. Nanosci. Nanotechnol.*, 2006, **6**(6), 1510–1532.

13 M. Aizawa, H. Iwase, T. Kamijo and A. Yamaguchi, Protein Condensation at Nanopore Entrances as Studied by Differential Scanning Calorimetry and Small-Angle Neutron Scattering, *J. Phys. Chem. Lett.*, 2022, **13**(37), 8684–8691.

14 H. Takahashi, *et al.*, Catalytic activity in organic solvents and stability of immobilized enzymes depend on the pore size and surface characteristics of mesoporous silica, *Chem. Mater.*, 2000, **12**, 3301–3305.

15 J. Larkin, R. Y. Henley, M. Muthukumar, J. K. Rosenstein and M. Wanunu, High-Bandwidth Protein Analysis Using Solid-State Nanopores, *Biophys. J.*, 2014, **106**, 696–704.

16 H. Chae, D. Kwak, M. Lee, S. Chi and K. Kim, Solid-state nanopore analysis on conformation change of p53TAD–MDM2 fusion protein induced by protein–protein interaction, *Nanoscale*, 2018, **10**(36), 17227–17235.

17 S. Alberti, *et al.*, Chemical Stability of Mesoporous Oxide Thin Film Electrodes under Electrochemical Cycling: From Dissolution to Stabilization, *Langmuir*, 2019, **35**, 6279–6287.

18 D. Grosso, *et al.*, Fundamentals of Mesostructuring Through Evaporation-Induced Self-Assembly, *Adv. Funct. Mater.*, 2004, **14**, 309–322.

19 A. Calvo, B. Yameen, F. J. Williams, G. J. A. A. Soler-Illia and O. Azzaroni, Mesoporous Films and Polymer Brushes Helping Each Other To Modulate Ionic Transport in Nanoconfined Environments. An Interesting Example of Synergism in Functional Hybrid Assemblies, *J. Am. Chem. Soc.*, 2009, **131**, 10866–10868.

20 L. Silies and A. Andrieu-Brunsen, Programming Ionic Pore Accessibility in Zwitterionic Polymer Modified Nanopores, *Langmuir*, 2018, **34**, 807–816.

21 S. Schmidt, S. Alberti, P. Vana, G. J. A. A. Soler-Illia and O. Azzaroni, Thermosensitive Cation-Selective Mesochannels: PNIPAM-Capped Mesoporous Thin Films as Bioinspired Interfacial Architectures with Concerted Functions, *Chem. – Eur. J.*, 2017, **23**, 14500–14506.

22 S. Alberti, J. Giussi, O. Azzaroni and G. J. A. A. Soler-Illia, A Comparative Study of PMETAC-Modified Mesoporous Silica and Titania Thin Films for Molecular Transport Manipulation, *Polymers*, 2022, **14**, 1–17.

23 H. Lim, *et al.*, Designed Patterning of Mesoporous Metal Films Based on Electrochemical Micelle Assembly Combined with Lithographical Techniques, *Small*, 2020, **16**, 1902934.

24 S. Alberti, G. J. A. A. Soler-Illia and O. Azzaroni, Gated supramolecular chemistry in hybrid mesoporous silica nanoarchitectures: controlled delivery and molecular transport in response to chemical, physical and biological stimuli, *Chem. Commun.*, 2015, **51**, 6050–6075.

25 P. Innocenzi and L. Malfatti, Mesoporous thin films: properties and applications, *Chem. Soc. Rev.*, 2013, **42**, 4198.

26 D. Huebner, *et al.*, Comparison of monomethoxy-, Dimethoxy-, and Trimethoxysilane anchor groups for surface-initiated RAFT polymerization from silica surfaces, *J. Polym. Sci., Part A: Polym. Chem.*, 2015, **53**, 103–113.

27 A. Vinu, K. Z. Hossain and K. Ariga, Recent Advances in Functionalization of Mesoporous Silica, *J. Nanosci. Nanotechnol.*, 2005, **5**, 347–371.

28 M. H. Lim and A. Stein, Comparative Studies of Grafting and Direct Syntheses of Inorganic−Organic Hybrid Mesoporous Materials, *Chem. Mater.*, 1999, **11**, 3285–3295.

29 C. Lee, T. Lin and C. Mou, Mesoporous materials for encapsulating enzymes, *Nano Today*, 2009, **4**(2), 165–179.

30 P. N. Catalano, A. Wolosiuk, G. J. A. A. Soler-illia and M. G. Bellino, Wired enzymes in mesoporous materials: A benchmark for fabricating biofuel cells, *Bioelectrochemistry*, 2015, **106**, 14–21.

31 C. M. Trouillefou, *et al.*, Protected activity of a phytase immobilized in mesoporous silica with benefits to plant phosphorus nutrition, *J. Sol-Gel Sci. Technol.*, 2015, **74**, 55–65.

32 J. Wei, New Insight into the Synthesis of Large-Pore Ordered Mesoporous Materials, *J. Am. Chem. Soc.*, 2017, **139**(5), 1706–1713.

33 J. Tu, *et al.*, Mesoporous Silica Nanoparticles with Large Pores for the Encapsulation and Release of Proteins, *ACS Appl. Mater. Interfaces*, 2016, **8**, 32211–32219.

34 P. Yang, *et al.*, Hierarchically Ordered Oxides, *Science*, 1998, **282**, 2244–2246.

35 C. J. Brinker, Y. Lu, A. Sellinger and H. Fan, Evaporation-induced self-assembly: Functional nanostructures made easy, *Adv. Mater.*, 1999, **11**, 579–585.

36 Y. Cheng, P. Müller-buschbaum and J. S. Gutmann, Ultrathin Anatase TiO 2 Films with Stable Vesicle Morphology Templated by PMMA- b - PEO, *Small*, 2007, **3**(8), 1379–1382.

37 G. J. a a Soler-Illia, *et al.*, Mesoporous hybrid and nanocomposite thin films. A sol–gel toolbox to create nanoconfined systems with localized chemical properties, *J. Sol-Gel Sci. Technol*, 2010, **57**, 299–312.

38 L. Malfatti, M. G. Bellino, P. Innocenzi and G. J. A. A Soler-Illia, One-Pot Route to Produce Hierarchically Porous Titania Thin Films by Controlled Self-Assembly, Swelling, and Phase Separation, *Chem. Mater.*, 2009, **21**(13), 2763–2769.

39 D. R. Ceratti, *et al.*, Critical effect of pore characteristics on capillary infiltration in mesoporous films, *Nanoscale*, 2015, **7**, 5371–5382.

40 P. C. Angelomé, M. C. Fuertes and G. J. A. A. Soler-Illia, Multifunctional, Multilayer, Multiscale: Integrative Synthesis of Complex Macroporous and Mesoporous Thin Films with Spatial Separation of Porosity and Function, *Adv. Mater.*, 2006, **18**, 2397–2402.

41 K. Matyjaszewski, Overview: Fundamentals of Controlled/Living Radical Polymerization, *ACS Symp. Ser.*, 1998, 2–30.

42 J. Zhang, Design of Amphiphilic ABC Triblock Copolymer for Templating Synthesis of Large-Pore Ordered Mesoporous Carbons with Tunable Pore Wall Thickness, *Chem. Mater.*, 2009, **21**(17), 3996–4005.

43 X. Tian, Recent advances in RAFT polymerization: Novel initiation mechanisms and optoelectronic applications, *Polymers*, 2018, **10**(3), 318.

44 R. T. Mayadunne, *et al.*, Living Radical Polymerization with Reversible Addition - Fragmentation Chain Transfer (RAFT Polymerization) Using Dithiocarbamates as Chain Transfer Agents, *Macromolecules*, 1999, **32**, 6977–6980.

45 Q. He, J. Shi, F. Chen, M. Zhu and L. Zhang, An anticancer drug delivery system based on surfactant-templated mesoporous silica nanoparticles, *Biomaterials*, 2010, **31**, 3335–3346.

46 A. Bertrand, *et al.*, Straightforward Preparation of Telechelic H-bonding Polymers From Difunctional Trithiocarbonates and Supramolecular Block Copolymers Thereof, *Macromolecules*, 2011, **44**, 3694–3704.

47 J. N. Israelachvili, *Intermolecular and Surface Forces*, Elsevier, 1992.

48 E. L. Crepaldi, *et al.*, Controlled Formation of Highly Organized Mesoporous Titania Thin Films: From Mesostructured Hybrids to Mesoporous Nanoanatase TiO$_2$, *J. Am. Chem. Soc.*, 2003, **125**, 9770–9786.

49 M. G. Bellino, A. E. Regazzoni and G. J. A. A. Soler-Illia, Amylase-Functionalized Mesoporous Silica Thin Films as Robust Biocatalyst Platforms, *ACS Appl. Mater. Interfaces*, 2010, **2**, 360–365.

50 M. G. Bellino, S. Municoy and G. J. A. A. Soler-illia, Enzymatic tandem systems engineered from mesoporous thin films: Synergy leading to efficient starch-electricity conversion, *Mater. Today Commun.*, 2016, **7**, 67–72.

51 B. A. Yu, Y. Wang, E. Barlow and F. Caruso, Mesoporous Silica Particles as Templates for Preparing Enzyme-Loaded Biocompatible Microcapsules, *Adv. Mater.*, 2005, **17**(14), 1737–1741.

52 J. Siefker, R. Biehl, M. Kruteva, A. Feoktystov and M. O. Coppens, Confinement Facilitated Protein Stabilization As Investigated by Small-Angle Neutron Scattering, *J. Am. Chem. Soc.*, 2018, **140**, 12720–12723.

53 R. Pogorilyi, *et al.*, Sol-Gel Derived Adsorbents with Enzymatic and Complexonate Functions for Complex Water Remediation, *Nanomaterials*, 2017, **7**, 298.

54 S. Alberti, E. Piccinini, P. G. Ramirez, G. S. Longo, M. Ceolin and O. Azzaroni, Mesoporous thin films on graphene FETs: nanofiltered, amplified and extended field-effect sensing, *Nanoscale*, 2021, **13**, 19098–19108.

55 H. Alem, F. Blondeau, K. Glinel, S. Demoustier-Champagne and A. M. Jonas, Layer-by-Layer Assembly of Polyelectrolytes in Nanopores, *Macromolecules*, 2007, **40**, 3366–3372.

56 L. S. Alberti Confinamiento como herramienta de diseño: Películas delgadas mesoporosas híbridas. (2018).

57 A. S. Angelatos, Y. Wang and F. Caruso, Probing the Conformation of Polyelectrolytes in Mesoporous Silica Spheres, *Langmuir*, 2008, **24**, 4224–4230.

58 T. D. Lazzara, K. H. A. Lau, A. I. Abou-Kandil, A.-M. Caminade, J.-P. Majoral and W. Knoll, Polyelectrolyte Layer-by-Layer Deposition in Cylindrical Nanopores, *ACS Nano*, 2010, **4**, 3909–3920.

59 Y. Wang, A. S. Angelatos, D. E. Dunstan and F. Caruso, Infiltration of Macromolecules into Nanoporous Silica Particles, *Macromolecules*, 2007, **40**(21), 7594–7600.

60 A. Yamaguchi, *et al.*, Structural Characterization of Proteins Adsorbed at Nanoporous Materials, *Anal. Sci.*, 2021, **37**, 49–59.

61 D. Grosso, *et al.*, Highly oriented 3D-hexagonal silica thin films produced with cetyltrimethylammonium bromide, *J. Mater. Chem.*, 2000, **10**, 2085–2089.

62 M. M. Zalduendo, *et al.*, Au Nanoparticles–Mesoporous TiO$_2$ Thin Films Composites as SERS Sensors: A Systematic Performance Analysis, *J. Phys. Chem. C*, 2018, **122**, 13095–13105.

63 C. Yu, M. Luo, F. Zeng, F. Zheng and S. Wu, Mesoporous silica particles for selective detection of dopamine with β-cyclodextrin as the selective barricade, *Chem. Commun.*, 2011, **47**, 9086–9088.

64 R. Luque and J. Garcia, From Mesoporous Supports to Mesoporous Catalysts: Introducing Functionality to Mesoporous Materials, *ChemCatChem*, 2013, **5**(4), 827–829.

65 J. C. Tom, C. Appel and A. Andrieu-brunsen, Soft Matter Fabrication and in situ functionalisation of mesoporous silica films by the physical entrapment of functional and responsive block copolymer structuring agents, *Soft Matter*, 2019, **15**(40), 8077–8083.